RSC Advances

PAPER

View Article Online
View Journal | View Issue

Cite this: *RSC Adv.*, 2017, **7**, 17244

Highly efficient red emission and multiple energy transfer properties of Dy^{3+}/Mn^{4+} co-doped $Ca_{14}Zn_6Ga_{10}O_{35}$ phosphors

Yiyang Zhou, Weiren Zhao,* Junhua Chen and Zifeng Liao

Received 20th February 2017
Accepted 12th March 2017

DOI: 10.1039/c7ra02112g

rsc.li/rsc-advances

Novel Dy^{3+}/Mn^{4+} co-doped $Ca_{14}Zn_6Ga_{10}O_{35}$ phosphors have been synthesized by a solid state reaction technique. Strong blue emission ranging from 370 nm to 500 nm was observed for the $Ca_{14}Zn_6Ga_{10}O_{35}$ host, attributed to the recombination of a donor–acceptor pair through a tunneling process. High internal and external quantum efficiencies of 64.4% and 56.2% respectively were obtained under the excitation of 310 nm in Mn^{4+} doped $Ca_{14}Zn_6Ga_{10}O_{35}$. This external quantum efficiency is the highest one reported for Mn^{4+} doped oxides. The temperature-dependent quantum efficiency of $Ca_{14}Zn_6Ga_{10}O_{35}:Mn^{4+}$ is also measured, indicating the unchanged absorption of the excitation light with temperature. In $Ca_{14}Zn_6Ga_{10}O_{35}:Dy^{3+}$, Mn^{4+} phosphors, multiple energy transfer from the host to Dy^{3+} and from Dy^{3+} to Mn^{4+} is observed and is confirmed to be a result of the dipole–dipole interaction. The emission changes from deep blue to white to deep red according to the different Dy^{3+}/Mn^{4+} concentration ratio, and the warm white emission can be realized with the chromaticity coordinate (0.345, 0.275), CCT 3525 K and CRI 87. These results suggest that $Ca_{14}Zn_6Ga_{10}O_{35}:Mn^{4+}$ phosphors have potential application as high efficiency red phosphors for solid-state lighting, while Dy^{3+}/Mn^{4+} co-doped $Ca_{14}Zn_6Ga_{10}O_{35}$ phosphors can be used as a single-phased white phosphor.

1 Introduction

The Mn^{4+} ion, which is similar to the isoelectronic Cr^{3+} (d^3), gives a rather complicated optical spectrum. It shows absorption in the whole ultraviolet region[1,2] and the subsequently emitted phosphorescence is in the deep red (620–720 nm) due to transition from the $^2E \rightarrow {}^4A_2$.[3,4] Thus, Mn^{4+}-doped red phosphors might have potential application in lighting,[5] holography,[6] lasers,[7] and dosimetry.[8]

As a kind of red phosphor with a high quantum efficiency, Mn^{4+} activated fluoride phosphors have attracted considerable interest.[9] Mn^{4+} doped K_2TiF_6 red phosphors show internal quantum yields as high as 98%, and high performance white LEDs with 3556 K correlated color temperature, 81 color rendering index (R_a) and luminous efficacy of 116 lm W^{-1} have been fabricated with these red phosphors.[10] Unfortunately, fluoride host is not stable because of their easy deliquescence.[11] Moreover, the toxic HF solution is harmful to the environment in the synthesis process, which restricts its applications. Fluoride phosphors are also not suitable for fluorescent lamps because of their reactivity with the mercury vapor.[12] Unlike fluoride phosphors, the Mn^{4+} activated oxide phosphors exhibit good chemical stability.[13] However, the currently known Mn^{4+} activated oxide phosphors cannot meet the needs of general lighting due to their low quantum efficiency. The internal quantum of $Sr_4Al_{14}O_{25}:Mn^{4+}$ and $3SrO{\cdot}5Al_2O_3:Mn^{4+}$ under 380 nm is close to 18%, 27% respectively.[14] The quantum efficiency of $La_2LiTaO_6:Mn^{4+}$, Mg^{2+} is 21.4%.[15] The internal and external quantum of $CaMg_2Al_{16}O_{27}:Mn^{4+}$ is 35.6% and 16.0% respectively.[16] The highest external quantum reported for Mn^{4+} doped phosphors is about 80% for $Sr_2MgAl_{22}O_{36}:Mn^{4+}$, but the internal quantum efficiency which is more important for application is still needed identification. Moreover, the synthesis temperature for $Sr_2MgAl_{22}O_{36}:Mn^{4+}$ as high as 1500 °C is not benefit for its application.[17] Therefore, Mn^{4+} activated oxide phosphors with high internal quantum efficiency under low synthesis temperature focused recently.[18]

It is known that Dy^{3+} ions exhibit characteristic emissions of the blue and yellow regions corresponding to $^4F_{9/2} \rightarrow {}^6H_{15/2}$ and $^4F_{9/2} \rightarrow {}^6H_{13/2}$ transitions under the excitation of NUV light, and thus result the emission of near white-light. Due to the overlap of the emission spectrum of Dy^{3+} ions and the excitation spectrum of Mn^{4+} ions, the energy transfer process between Dy^{3+} ions and Mn^{4+} ions can be expected based on Dexter's energy transfer theory.[19] Therefore, it is reasonable to believe Dy^{3+}/Mn^{4+} co-doped samples possess higher color rendering index (CRI) and lower color temperature than the single Dy^{3+}-doped samples.

In our work, photoluminescence properties of Mn^{4+} doped and Mn^{4+}/Dy^{3+} co-doped $Ca_{14}Zn_6Ga_{10}O_{35}$ (CZGO) are studies.

School of Physics and Optoelectronic Engineering Guangdong University of Technology, Guangzhou 510006, China. E-mail: zwren123@126.com; Fax: +86 020 39322265; Tel: +86 020 39322265

The intense blue light emission of CZGO host was observed for first time. High quantum efficiency for Mn^{4+} doped CZGO was obtained. The internal and external quantum efficiencies of $Ca_{14}Zn_6Ga_{9.85}O_{35}$:0.15$Mn^{4+}$ synthesized under 1210 °C reached 64.4% and 56.2%, the highest external quantum efficiency in Mn^{4+} activated oxide phosphors reported according to our knowledge. For Dy^{3+}/Mn^{4+} co-doped CZGO, the CIE chromaticity coordinate (0.345, 0.275), color rendering index (CRI) 85 and color temperature 3525 K are obtained. Moreover, multiply energy transfer processes have been observed and discussed by Inokuti–Hirayama (I–H) model and Dexter's theory. The results show that Mn^{4+} doped CZGO is a potential red phosphor for high performance white light LED devices.

2 Experiment

2.1 Material synthesis

$Ca_{14-x}Zn_6Ga_{10-y}O_{35}$:$xDy^{3+}$, yMn^{4+} (x = 0–0.18, y = 0–0.25) were prepared by the solid-state reaction method. $CaCO_3$ (99.9% purity), ZnO (99.9% purity), Ga_2O_3 (99.9% purity), Dy_2O_3 (99.99% purity) and MnO_2 (99.99% purity) were used as the starting reactants. According to the stoichiometric composition, the reactants were weighed and mixed thoroughly in an agate mortar, then sintered in a tubular furnace at 1210 °C for 6 h in air. After cooled down to the room temperature, the synthetic products were ground for subsequent analysis.

2.2 Characterizations

The phase compositions of the synthesized samples were studied using an Ultima IV X-ray diffractometer with Cu Kα radiation (λ = 1.5406 Å) operated at 36 kV tube voltage and 20 mA tube current. The morphology of the samples were characterized using a S3400N scanning electron microscope (SEM). The PL spectra were obtained using a Hitachi F-7000 spectrophotometer at room temperature with a Xe lamp as source. Time-resolved photoluminescence decays were recorded by a FLS980 (Edinburgh) time-correlated single-photon counting (TCSPC) spectrofluorometer using an interchangeable Nano LED source for excitation. The temperature dependence of luminescence and photoluminescence quantum yields were measured by an Olsuka Electronics QE-2100 intensified multichannel spectrometer.

3 Results and discussion

3.1 XRD and SEM analysis

Fig. 1(a) shows the X-ray diffraction (XRD) patterns of $Ca_{14-x}Zn_6Ga_{10-y}O_{35}$:$xDy^{3+}$, yMn^{4+} (x, y = 0, 0; 0.1, 0; 0, 0.12; 0.1, 0.12). All patterns of the samples are well in agreement with the standard XRD pattern of CZGO (#245649).[20] Fig. 1(b) shows the unit cells viewed from [100] for CZGO crystal which possesses cubic structure with space group $F23$ (196) and lattice parameters a = 15.0794 Å and V = 3428.88 Å^3. In the crystal lattice of CZGO, tetrahedral GaO_4 and ZnO_4 (partial disorder) share vertices to form a 3D network with two types of large empties. One type of these empties is filled with octahedral (Ga, Zn)O_6^{-}, while the other ones are half occupied by four corner-linked tetrahedral ZnO_4 sharing common oxygen atom, according to Pauling's rules.[21] On the basis of the effective ionic radii of cation with different coordination numbers (CN),[22] Dy^{3+} (6CN, 0.91 Å; 7CN, 0.97 Å) ions are expected to randomly occupy six- and seven-coordinated Ca^{2+} (6CN, 1.00 Å; 7CN, 1.06 Å) sites, and Mn^{4+} (6CN, 0.53 Å) ions are preferentially accommodated at the Ga^{3+} (6CN, 0.62 Å) sites with an octahedral coordination in the crystal structure.

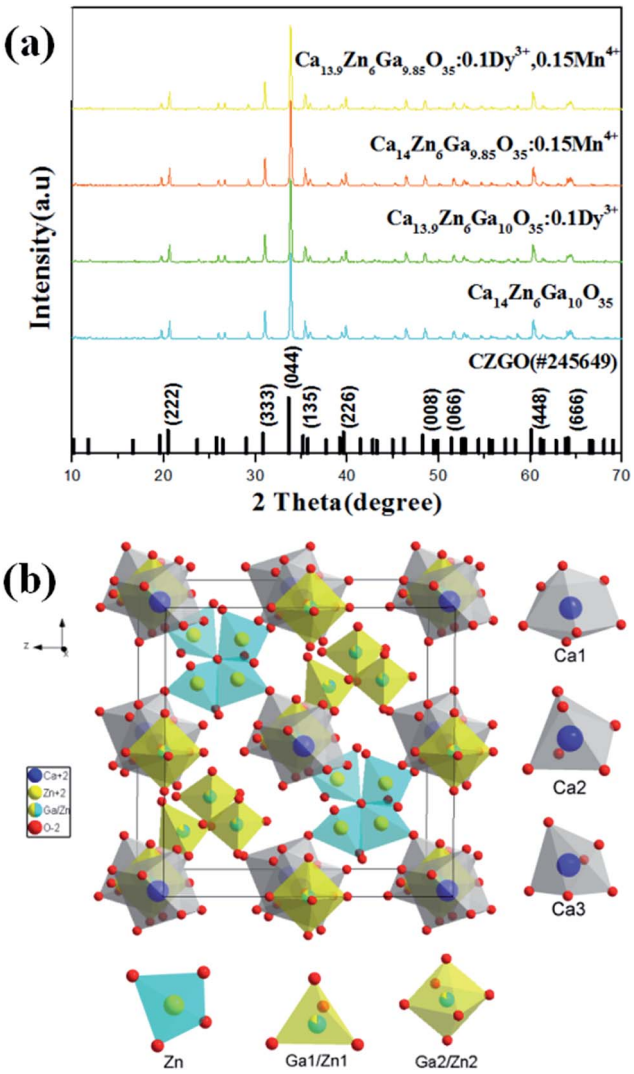

Fig. 1 (a) XRD patterns of $Ca_{14-x}Zn_6Ga_{10-y}O_{35}$:$xDy^{3+}$, yMn^{4+} (x, y = 0, 0; 0.1, 0; 0, 0.15; 0.1, 0.15). (b) A schematic of the CZGO crystal structure viewed in x-direction.

Fig. 2 displays the SEM image of $Ca_{13.9}Zn_6Ga_{9.85}O_{35}$:0.1$Dy^{3+}$, 0.15$Mn^{4+}$. The sample exhibits non-identical grains with the particle size approximately sub-micrometer to a few micrometers which tend to aggregate.

3.2 High PL QEs of CZGO:Mn^{4+}

Fig. 3(a) shows the diffuse reflection spectra of $Ca_{14}Zn_6Ga_{10-y}O_{35}$:$yMn^{4+}$ (y = 0.00, 0.03, 0.12, and 0.25). There are three dips of reflectivity between 280 and 550 nm. Two dips locating at 332 and 465 nm are assigned to strong spin-allowed transitions in

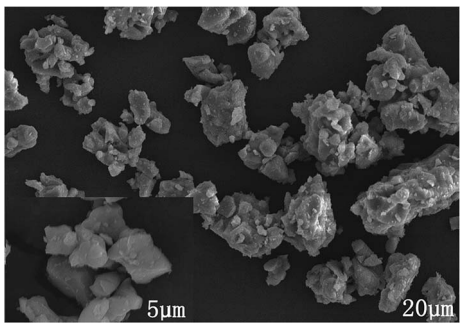

Fig. 2 SEM image of $Ca_{13.9}Zn_6Ga_{9.85}O_{35}$:0.1$Dy^{3+}$, 0.15$Mn^{4+}$ sample.

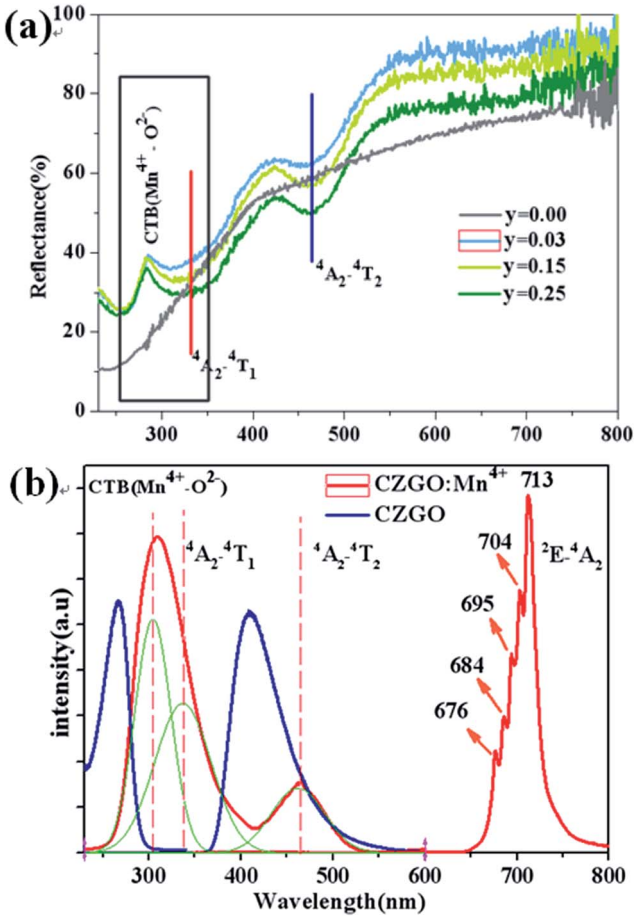

Fig. 3 (a) Representative diffuse reflection spectra of $Ca_{14}Zn_6Ga_{10-y}O_{35}$:$yMn^{4+}$ (y = 0.00, 0.03, 0.12, 0.25). (b) PLE and PL of CZGO (λ_{em} = 410 nm, λ_{ex} = 266 nm) and $Ca_{14}Zn_6Ga_{9.99}O_{35}$:0.01$Mn^{4+}$ (λ_{em} = 713 nm, λ_{ex} = 310 nm).

Mn^{4+} ions corresponding to $^4A_2 \rightarrow {}^4T_2$ and $^4A_2 \rightarrow {}^4T_1$, respectively. The broad dip in the range of 250–350 nm is aroused by both Mn^{4+}–O^{2-} charge transfer transition and $^4A_2 \rightarrow {}^4T_1$ transition of Mn^{4+} ions, which can be judged from the excitation spectra as below.

PLE and PL of CZGO (λ_{em} = 410 nm, λ_{ex} = 266 nm) and $Ca_{14}Zn_6Ga_{9.99}O_{35}$:0.01$Mn^{4+}$ (λ_{em} = 713 nm, λ_{ex} = 310 nm) are shown in Fig. 3(b). For CZGO, an absorption band from about 200 nm to 300 nm centered at 266 nm (monitored emission wavelength λ_{em} = 410 nm) and a broad-band PL blue emission centered at 410 nm extend from 360 nm to 500 nm (excitation wavelength λ_{ex} = 266 nm) of CZGO are observed. The broad-band blue emission has not been reported in CZGO before,[19,20] but similar blue emission was observed in $ZnGa_2O_4$ crystals owning to the distorted octahedral Ga–O groups serving as the self-activated luminescent centers.[23–27] It is reasonable to ascribe the broad-band blue emission to the recombination of a donor–acceptor pair (DAP) through a tunneling process in CZGO host. For $Ca_{14}Zn_6Ga_{9.97}O_{35}$:0.03$Mn^{4+}$, the excitation spectrum can be fitted by three Gaussian curves, leading to three distinguished bands peaking at 303 (band I, 33 003 cm^{-1}), 332 (band II, 30 120 cm^{-1}) and 465 (band III, 21 505 cm^{-1}) which are in good agreement with those in the diffuse reflection spectra. The excitation bands located at 332 and 465 nm are assigned to the spin-allowed ($^4A_2 \rightarrow {}^4T_2$) and ($^4A_2 \rightarrow {}^4T_1$) transitions of Mn^{4+}, respectively. The broad band, which is composed by bands I and II, is due to the overlap between the transitions of Mn^{4+}–O^{2-} and the spin-allowed transitions of Mn^{4+} ($^4A_2 \rightarrow {}^4T_1$). Under excitation at 310 nm, the intense red emission is composed of some distinguishable sharp R lines and Stokes/anti-Stokes side-peaks, located at 676, 684, 695, 704 and 713 nm, due to different vibrational modes for the $3d^3$ electrons when Mn^{4+} is of the octahedral complex.[28] Although there is an overlap between the PLE spectrum of CZGO and Mn^{4+} ion, our measurement for the average lifetimes of the PL spectrum of CZGO with different Mn^{4+} concentration suggesting there is no energy transfer between CZGO and Mn^{4+}.

The energy splitting of Mn^{4+} ion with octahedral coordination on the crystal field strength can be well illustrated by Tanabe–Sugano energy diagram (Fig. 4).[29] The value of the local crystal-field parameter D_q can be obtained from the peak energy (21 505 cm^{-1}) of the $^4A_2 \rightarrow {}^4T_2$ transition[30]

$$D_q = E(^4A_{2g} \rightarrow {}^4T_{2g})/10 \quad (1)$$

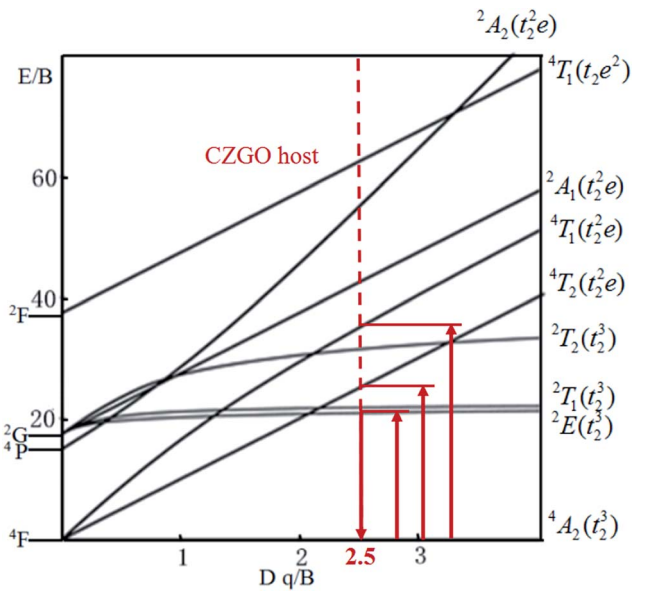

Fig. 4 Tanabe–Sugano diagram for Mn^{4+} in CZGO.

Moreover, based on the obtained energy difference (8615 cm^{-1}) between the $^4A_2 \rightarrow {}^4T_2$ and $^4A_2 \rightarrow {}^4T_1$ transitions, Racah parameter B can be evaluated from the expression[31]

$$\frac{D_q}{B} = \frac{15(x-8)}{(x^2-10x)} \quad (2)$$

here the parameter x is defined as

$$x = \frac{E\left({}^4A_1 \rightarrow {}^4T_1\right) - E\left({}^4A_1 \rightarrow {}^4T_2\right)}{D_q} \quad (3)$$

According to the peak energy (14 025 cm^{-1}) corresponding to $^2E \rightarrow {}^4A_2$ transition of Mn^{4+} derived from emission spectrum above, Racah parameter C can be calculated by the following eqn[32]

$$E(^2E \rightarrow {}^2A_2)/B = 3.05C/B + 7.9 - 1.8B/D_q \quad (4)$$

The values of D_q, B and C in the CZGO:Dy^{3+}, Mn^{4+} are then determined to be 2150, 860 and 2572 cm^{-1}, respectively. The values of B is higher than those reported in oxides while the values of C is smaller than those reported in oxides, and the values of D_q is similar to those reported in oxides.[33] In fact, the emission peak energy of $^2E \rightarrow {}^4A_2$ transition is singularly dependent on the covalence of the "Mn^{4+}–ligand" bonding (nephelauxetic effect). The nephelauxetic ratio β can be determined by following equation:[34]

$$\beta = \sqrt{(B/B_0)^2 + (C/C_0)^2} \quad (5)$$

here B_0 and C_0 represent Racah parameters for free ions. For Mn^{4+} ions, B_0 and C_0 are equal to 1160 cm^{-1} and 4303 cm^{-1}, respectively.[35] So β for Mn^{4+} in CZGO is calculated to be 0.952. This value is similar to those reported in oxides, but higher than those in fluorides, due to the more ionic Mn^{4+}–F^- bonding than Mn^{4+}–O^{2-} bonding.[36]

Fig. 5 shows PL spectra (λ_{ex} = 310 nm) of $Ca_{14}Zn_6Ga_{10-y}O_{35}$:$yMn^{4+}$ phosphors as a function of y at room temperature. The PL intensity of Mn^{4+} ions increases with increased Mn^{4+} concentration, and concentration quenching occurs beyond y = 0.15. Photoluminescence internal and external quantum efficiency of $Ca_{14}Zn_6Ga_{10-y}O_{35}$:$yMn^{4+}$ phosphors is measured in Table 1. The photoluminescence internal an external quantum efficiencies (QEs) reach 64.4% and 56.2% respectively when y = 0.15. Although the internal quantum efficiency of our sample is lower than the phosphor $Sr_2MgAl_{22}O_{36}$:Mn^{4+} reported by Renping Cao,[17] the external quantum efficiency of our sample has been the highest one according to our knowledge.

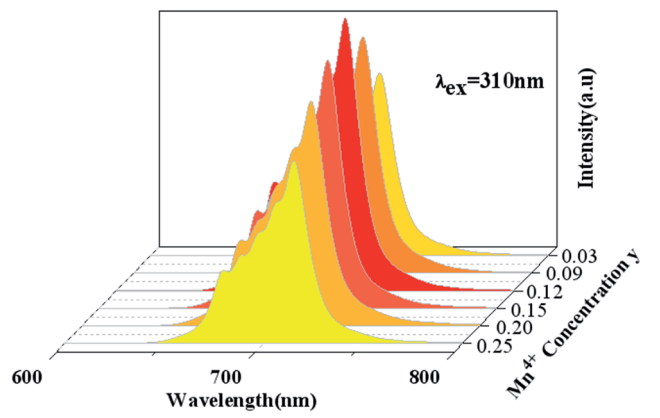

Fig. 5 Photoluminescence emission spectra of $Ca_{14}Zn_6Ga_{10-y}O_{35}$:$yMn^{4+}$ (y = 0.03, 0.09, 0.12, 0.15, 0.20, 0.25) under λ_{ex} = 310 nm.

The temperature-dependent emission spectra is shown in Fig. 6, and two features can be observed: (1) emission intensity decreases with temperature increasing (2) all emission peaks shift to longer wavelength (red shift) region with increasing temperature.

The Arrhenius equation can be used to evaluate activation energy ΔE for thermal quenching:[37]

$$I_T = I_0/[1 + c\exp(-\Delta E/kT)] \quad (6)$$

here I_0 is the initial emission intensity, I_T is the intensity at temperature T, c is a constant, k is the Boltzmann constant, and ΔE is the activation energy for thermal quenching. Based on the PL spectra in Fig. 6, the ΔE of CZGO:Mn^{4+} is obtained as 0.156 eV by fitting the curve of $\ln[(I_0/I_T) - 1]$ *versus* $1/kT$, as shown in the inset of Fig. 6.

The peak position, the internal and external QEs are shown in Table 2. The peak position shifts from 713.4 to 716.6 nm as temperature from 298 K to 573 K. The red-shift behavior can be

Table 1 Photoluminescence internal and external QEs at different y in $Ca_{14}Zn_6Ga_{10-y}O_{35}$:$yMn^{4+}$ phosphors excited at 310 nm

y	0.03	0.09	0.12	0.15	0.20	0.25
Internal QE (%)	41.3	49.5	59.4	64.4	54.6	44.6
External QE (%)	36.2	43.7	52.4	56.2	48.2	38.3

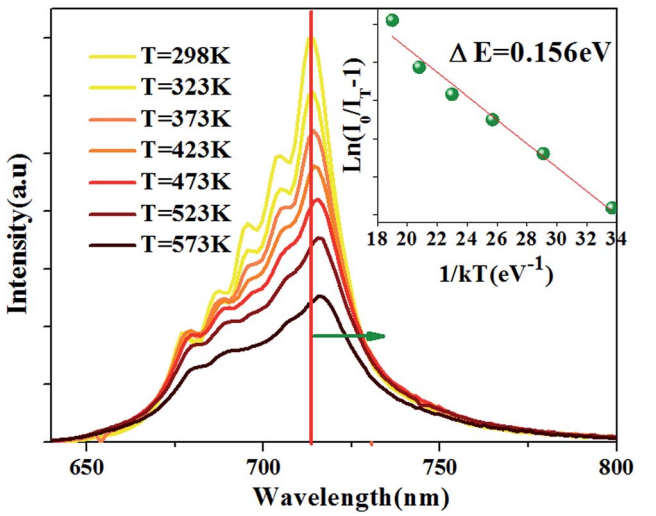

Fig. 6 PL spectra at different temperature for the $Ca_{14}Zn_6Ga_{9.85}O_{35}$:$0.15Mn^{4+}$ excited at 310 nm. The inset: the activation energy 0.156 eV for $Ca_{14}Zn_6Ga_{9.85}O_{35}$:$0.15Mn^{4+}$.

Table 2 The peak position, internal and external QEs of $Ca_{14}Zn_6Ga_{9.85}O_{35}$:0.15$Mn^{4+}$ at different temperature

Temperature (K)	298	323	373	423	473	523	573
Peak (nm)	713.4	714.0	714.3	715.0	715.6	715.9	716.6
Internal QE (%)	64.4	63.7	61.4	59.4	56.4	53.0	45.9
External QE (%)	56.2	55.4	53.4	51.6	49.0	46.1	39.9

explained by the Varshini equation for temperature dependence[38,39]

$$E(T) = E_0 - \frac{aT^2}{T+b} \quad (7)$$

where $E(T)$ is the energy difference between excited states and ground states at a temperature T, E_0 is the energy difference at 0 K, and a and b are fitting parameters. The bond lengths between the luminescent center and its ligand ions increase with increased temperature, which results in the decreased crystal field. Then, it will cause the split of degenerate excited state or ground state, resulting in the decrease of the transition energy. Therefore, the emission peak is red-shifted with the increase of temperature.[40] The red-shift behavior can also be explained by Tanabe–Sugano energy diagram (Fig. 4), decreased crystal field correspond to less value of D_q/B, resulting in the smaller transition energy between excited state ^2E and ground state $^4A_2$.

Both internal QE and external QE decreases with increased temperature. The internal and external QEs decrease 28.7% and 29.0% of the values at 298 K, respectively. Almost the same decreasing rate indicates that the change of QEs with temperature is not brought by the change of the absorption of the incident light on the phosphors.

3.3 White light of CZGO:Dy^{3+}

Fig. 7 displays the PL and PLE spectra of $Ca_{13.9}Zn_6Ga_{10}O_{35}$:0.1$Dy^{3+}$ (λ_{em} = 410 nm and 486 nm, λ_{ex} = 266 nm and 352 nm). The broad emission blue band centered at 410 nm is obviously from CTB of host. The absorption peak centered at 352 nm and the sharp emission bands centered at 486 nm and 578 nm come from the transition $^6H_{15/2} \rightarrow {}^6P_{7/2}$, $^4F_{9/2} \rightarrow {}^6H_{13/2}$ and $^4F_{9/2} \rightarrow {}^6H_{15/2}$ for Dy^{3+} ion respectively. It can be seen that the emission spectrum under the excitation 266 nm have the similar profile with that excited at 352 nm except for the appearance of the wide band centered at 410 nm. In addition to, the intensity of emission excited at 266 nm is much times higher than the emission excited at 352 nm, which indicating the high photon energy that host absorbed can be transferred efficiently to Dy^{3+} ion.

The dependence of the emission host intensities of $Ca_{14-x}Zn_6Ga_{10}O_{35}$:$x$$Dy^{3+}$ phosphors on Dy^{3+} concentration x is shown in Fig. 8. The change of the intensity for $^4F_{9/2} \rightarrow {}^6H_{13/2}$, $^6H_{15/2}$ transition shows the feature of concentration quenching with the maximum intensity as x = 0.1. However, the blue intensity for host decreases monotonically with x increase, indicating further the existence of the energy transfer from the host to Dy^{3+} ions.

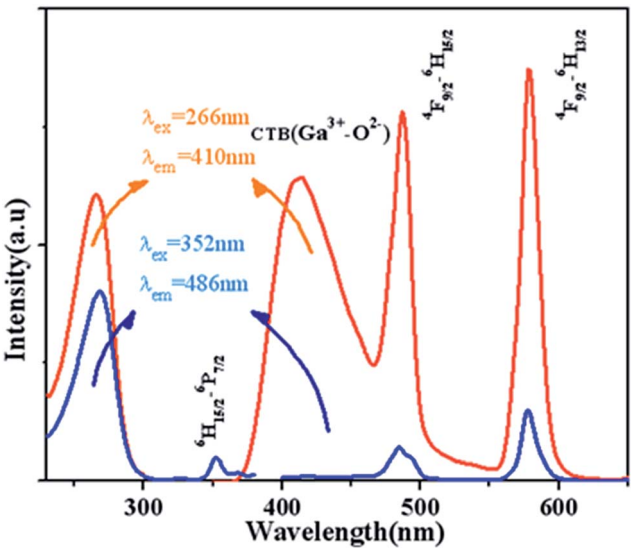

Fig. 7 PL and PLE spectra of $Ca_{13.9}Zn_6Ga_{10}O_{35}$:0.1$Dy^{3+}$ (λ_{em} = 410 nm and 486 nm, λ_{ex} = 266 nm and 352 nm).

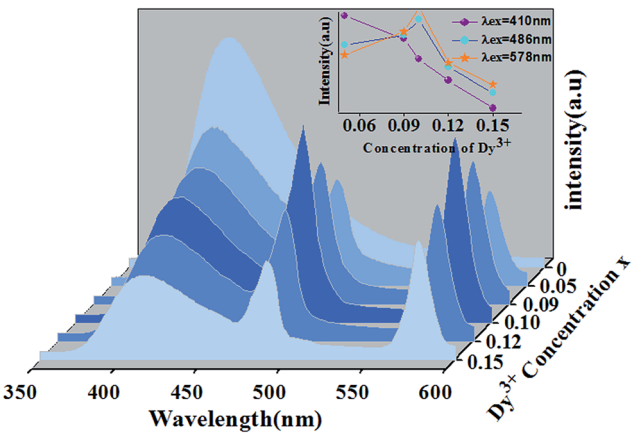

Fig. 8 Emission spectra of $Ca_{14-x}Zn_6Ga_{10}O_{35}$:$x$$Dy^{3+}$ under the excitation of 266 nm. The inset shows the dependence of three emission peakshost on Dy^{3+} concentration.

An energy band diagram is proposed in Fig. 9. The broad-band blue emission of host is suggested to be ascribed to the recombination of a donor–acceptor pair (DAP) through a tunneling process, that is, from the transition between electrons trapped by the donor band (DB) (being formed by oxygen vacancies) and holes captured by the acceptor band (AB) (being formed by gallium vacancy) (V_{Ga}), or pair of gallium vacancy and oxygen vacancy (V_O, V_{Ga}). It is worth noting that the absorption energy (4.7 eV, 266 nm) of host is located at approximately twice the energy of the Dy^{3+}:$^4F_{9/2} \rightarrow {}^6H_{13/2}$ (2.1 eV, 578 nm) or $^4F_{9/2} \rightarrow {}^6H_{15/2}$ (2.5 eV, 486 nm) transition. Moreover, absorption bands of the host and Dy^{3+} are almost overlapped in Fig. 7, which means the energy transfer process from the host to Dy^{3+} is dominated by the cooperative energy transfer.[41,42] The cooperative energy transfer between the CZGO host and Dy^{3+} ions can be understood as following: in first step, the electrons in the

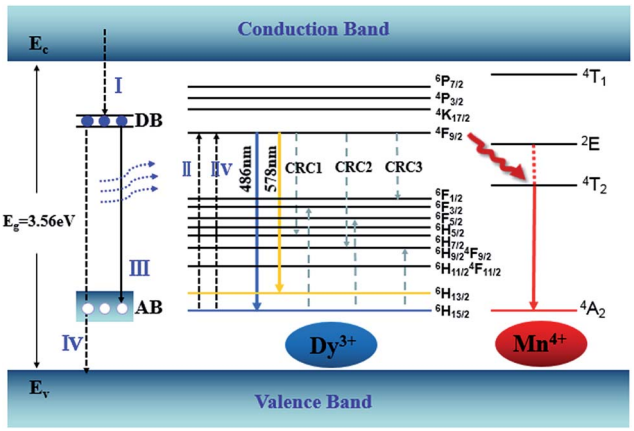

Fig. 9 Energy level diagram showing energy transfer and the CR processes of CZGO:Dy^{3+}, Mn^{4+}.

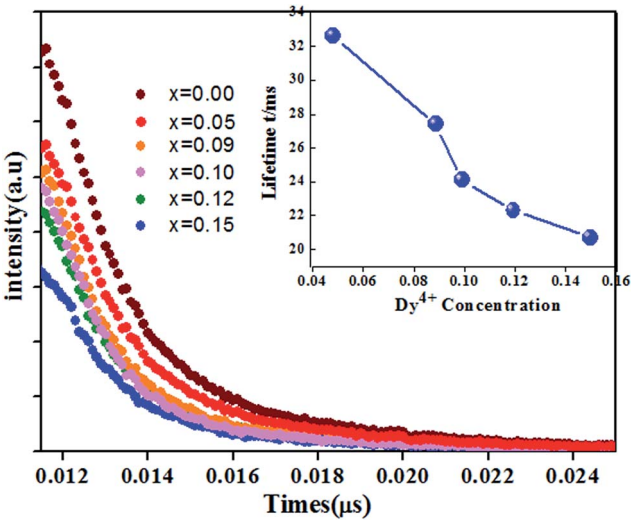

Fig. 10 Luminescence decay curves of $Ca_{14-x}Zn_6Ga_{9.88}O_{35}$:$xDy^{3+}$ (x = 0.00, 0.05, 0.09, 0.10, 0.12, 0.15) (monitored at 410 nm excited at 266 nm). The inset: dependence of the lifetime τ and energy transfer efficiency η on Dy^{3+} doping concentration.

conduction band de-excite to DB (process I in Fig. 9), accompanying the excitation of Dy^{3+} from $^6H_{15/2}$ to $^4F_{9/2}$ (process II in Fig. 9) followed by the emission of Dy^{3+} ($^4F_{9/2} \rightarrow {}^6H_{13/2}$ and $^4F_{9/2} \rightarrow {}^6H_{15/2}$); In second step, the electrons in DB can either de-excite to AB (process III in Fig. 9) which results the emission of the host, or to valance band (process IV in Fig. 9) which results the excitation of Dy^{3+} from $^6H_{15/2}$ to $^4F_{9/2}$ (process IIV in Fig. 9) followed by the emission of Dy^{3+}. The concentration quenching of Dy^{3+} emission intensity can be ascribed to the cross relaxation between neighboring Dy^{3+} ions. Cross relaxation (CR) occurs when the energy from excited states promotes the ground state to the metastable levels. For Dy^{3+} ions, the CR mechanisms [$^4F_{9/2}$, $^6H_{15/2}$] $\rightarrow$ [$^6H_{7/2}/^4F_{9/2}$, $^6F_{3/2}$], [$^4F_{9/2}$, $^6H_{15/2}$] $\rightarrow$ [$^6H_{9/2}/^6F_{11/2}$, $^6F_{5/2}$] and [$^4F_{9/2}$, $^6H_{15/2}$] $\rightarrow$ [$^6F_{1/2}$, $^6H_{9/2}/^6F_{11/2}$] denoted by CRC1, CRC2, and CRC3, respectively, are possible responsible to the concentration quenching based on the energy match rule, as illustrated in Fig. 9.

The fluorescence decay curves of $Ca_{14-x}Zn_6Ga_{10}O_{35}$:$xDy^{3+}$ (x = 0.00, 0.05, 0.09, 0.10, 0.12, 0.15) monitored at 410 nm with the excitation of 266 nm are shown in Fig. 11. The curve can be nearly fitted by one exponential function, and the average lifetime τ is given by[43]

$$\tau = \int_0^\infty tI(t)\mathrm{d}t \Big/ \int_0^\infty I(t)\mathrm{d}t \tag{8}$$

where $I(t)$ is the luminescent intensity at time t. The obtained τ is given in the inset of Fig. 10. The lifetime decreased from 32.8 μs to 22.6 μs when the concentration of Dy^{3+} increased from 0.05 to 0.15. The decrease of lifetime with increase of Dy^{3+} concentration confirms the existence of the energy transfer between host and Dy^{3+} ions.

In order to figure out the interaction type of energy transfer between host and Dy^{3+} ions, the donor centers of oxygen vacancies marked as "A", are considered. If "A" and Dy^{3+} ions are randomly distributed in the host and the migration processes among Dy^{3+} ions are negligible, then the temporal evolution of the Dy^{3+} luminescence intensity $I(t)$, following pulsed excitation at 266 nm, can be given by the Inokuti–Hirayama (I–H) model[44]

$$I(t) = I(0)\exp\left(-\frac{t}{\tau_0} - \gamma t^{\frac{3}{S}}\right) \tag{9}$$

where $I(0)$ is luminescence intensity when $t = 0$, τ_0 is the lifetime of the host in the absence of Dy^{3+} ions, S is the multipolar interaction parameter, and the energy transfer parameter γ is defined by

$$\gamma = \frac{4\pi}{3}C_A\Gamma\left(1 - \frac{3}{S}\right)\left(C_{DA}{}^{(S)}\right)^{\frac{3}{S}} \tag{10}$$

in which C_A is Dy^{3+} concentration, $\Gamma(x)$ is the gamma function, and $C_{DA}{}^{(S)}$ is the "A" $\rightarrow$ Dy^{3+} energy transfer parameter. The decay curves for the samples doped with 5 mol% and 10 mol% of Dy^{3+} ions are presented in Fig. 11. The best fitting using I–H model is $S = 6$, indicating the energy transfer between the host and Dy^{3+} ions is dominantly governed by dipole–dipole interaction.

Considering no overlap between PLE and PL spectra of Dy^{3+}, the concentration quenching of Dy^{3+} emission cannot be related to the radiation re-absorption. It might be attributed to multipole–multipole interaction or exchange interaction. In order to figure out this point, the average distance (R_c) between the nearest Dy^{3+} ions can roughly be calculated using the following eqn.[45]

$$R_C \approx 2\left[\frac{3V}{4\pi X_c N}\right]^{\frac{1}{3}} \tag{11}$$

where V is the volume of the unit cell; N is the number of host cations which can be replaced by Dy^{3+} ions in the unit cell; X_c is the critical concentration of Dy^{3+} ion. For this case, $V = 3428.88$ Å^3, $N = 4$, $X_c = 0.10$, R_c is obtained to be 25 Å. Blasse[46] has pointed out that multipolar interaction predominates if R_c is larger than 5 Å. Therefore, the multipolar interaction accounts for the concentration quenching in CZGO:Dy^{3+} phosphors.

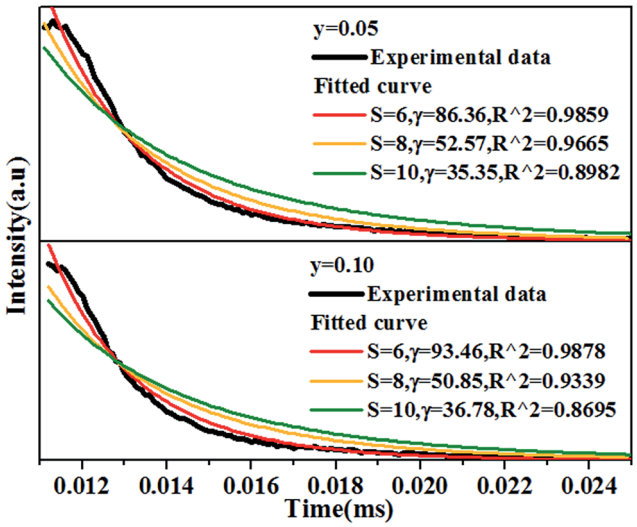

Fig. 11 Decay curves of $Ca_{14-x}Zn_6Ga_{10}O_{35}$:$xDy^{3+}$, ($x$ = 0.05, 0.10) measured by 266 nm excitation and monitored at 410 nm, together with the fitted curves using I–H model, showing the best fitting when S = 6. All the experimental data of samples.

Based on the model proposed by Dexter,[47] the interaction type between Dy^{3+} ions can be identified by

$$I/x = [1 + \beta(x)^{\theta/3}]^{-1} \quad (12)$$

where I is the emission intensity of Dy^{3+} ion under the excitation of 352 nm; x is Dy^{3+} concentration; and is a constant for the same excitation condition for a given host. θ = 6, 8, or 10 for dipole–dipole (d–d), dipole–quadrupole (d–q) and quadrupole–quadrupole (q–q), respectively. For the phosphor CZGO:Dy^{3+}, the dependence of $\log(I/x_{Dy^{3+}})$ on $\log(x_{Dy^{3+}})$ shown in Fig. 12 is almost linear and the fitted line slopes are −1.44 and −1.49 for $^4F_{9/2} \rightarrow {}^6H_{13/2}$ and $^4F_{9/2} \rightarrow {}^6H_{15/2}$ transition respectively. The value of θ is 6 determined by the line slope, indicating the electric d–d interaction is responsible for the concentration quenching of Dy^{3+} ions in CZGO.

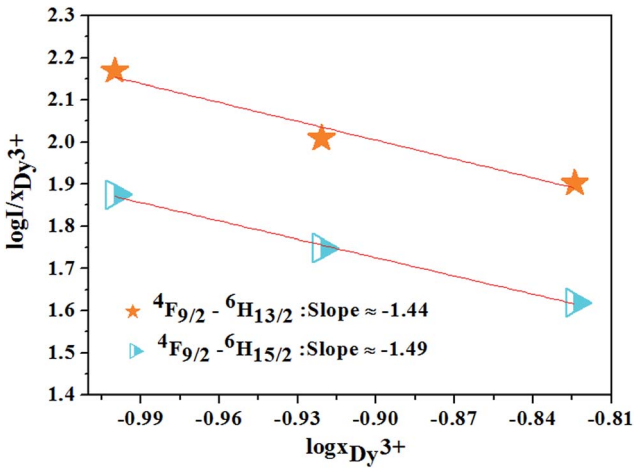

Fig. 12 The relations of $\log(I/x_{Dy^{3+}})$ and $\log(x_{Dy^{3+}})$ for $^4F_{9/2} \rightarrow {}^6H_{13/2}$, $^4F_{9/2} \rightarrow {}^6H_{15/2}$ transitions of Dy^{3+} ions.

3.4 Optimized white light of CAGO:Dy^{3+}, Mn^{4+}

Fig. 13 shows PL spectra of $Ca_{13.9}Zn_6Ga_{10-y}O_{35}$:0.1$Dy^{3+}$, yMn^{4+} phosphors (y = 0.03, 0.09, 0.12, 0.15, 0.20, 0.25) at room temperature (λ_{ex} = 266 nm). The spectra exhibits blue CTB, blue/yellow emissions and a deep red emission, which result from the emission of host, $^4F_{9/2} \rightarrow {}^6H_{15/2}/{}^4F_{9/2} \rightarrow {}^6H_{13/2}$ transitions of Dy^{3+} ion and $^2E \rightarrow {}^4A_2$ transition of Mn^{4+} ion, respectively. As Mn^{4+} concentration increases, the emissions intensity of both host and Dy^{3+} ions decrease, and the maximum emission of Mn^{4+} ions is shown as y = 0.15. As discussed above, energy transfer exists from host to Dy^{3+} ions at the excitation of 266 nm. Moreover, the external QEs of Mn^{4+} ion excited at 266 nm in $Ca_{13.9}Zn_6Ga_{9.85}O_{35}$:0.1$Dy^{3+}$, 0.15$Mn^{4+}$ and $Ca_{14}Zn_6Ga_{9.85}O_{35}$:0.15$Mn^{4+}$ are measured as 15.6% and 10.1%, which indicating the energy transfer from Dy^{3+} to Mn^{4+} helps enhancing the QEs of Mn^{4+} emission. Energy transfer from Dy^{3+} to Mn^{4+} ions is also possible due to the overlap between the PLE spectrum of Mn^{4+} ions and PL spectrum of Dy^{3+} ions in CAGO:Dy^{3+}, Mn^{4+}. The energy transfer mechanism from Dy^{3+} to Mn^{4+} ion can be explained as non-radiative transitions from $^4F_{9/2}$ level of Dy^{3+} (20 747 cm^{-1}) to $^4T_2$ level of Mn^{4+} (14 025 cm^{-1}) by the assistance of phonons[48] by Fig. 10. Therefore, multiply energy transfer can be happen in CZGO:Dy^{3+}, Mn^{4+} at the excitation of 266 nm.

Fig. 14(a) shows the luminescence decay curves (excited at 266 nm and monitored at 486 nm of Dy^{3+} emission) of $Ca_{13.9}Zn_6Ga_{10-y}O_{35}$:0.1$Dy^{3+}$, yMn^{4+} samples. The lifetimes were determined by the fitting of single exponential function to be 0.630, 0.468, 0.360, 0.334, 0.316, 0.296 and 0.261 ms for y = 0, 0.03, 0.09, 0.12, 0.15, 0.20, and 0.25 respectively, shown also in Fig. 14(a). The decrease of the lifetime confirms the existence of energy transfer from Dy^{3+} to Mn^{4+}. The energy-transfer efficiency η_T is calculated using eqn (5) and shown in Fig. 14(b). Although the value of η_T always increase with increasing Mn^{4+} dopant concentration in our experiment, the emission intensity of Mn^{4+} tends to decrease at higher Mn^{4+} concentration (x > 0.15) due to the concentration quenching. The energy transfer efficiency is 59% when y = 0.25 with maximal 713 nm emission intensity.

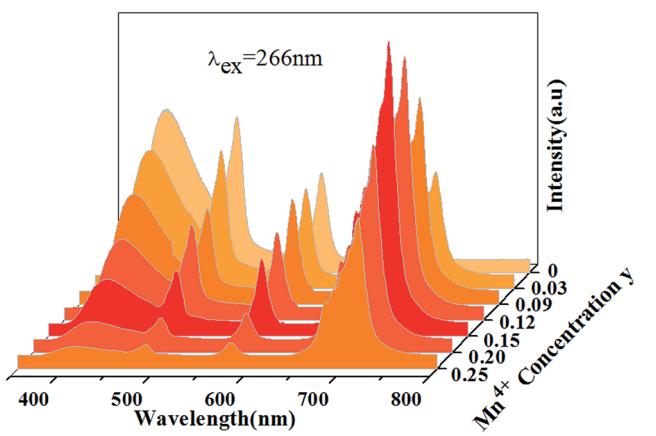

Fig. 13 Photoluminescence emission spectra of $Ca_{13.9}Zn_6Ga_{10-y}O_{35}$:0.1$Dy^{3+}$, yMn^{4+} as a function of y under λ_{ex} = 266 nm.

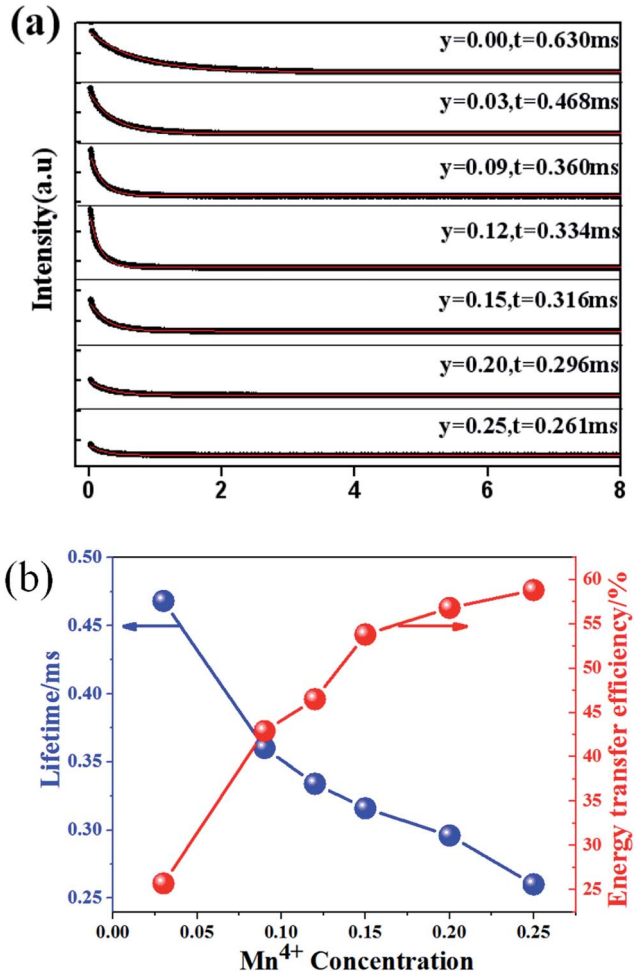

Fig. 14 (a) Decay curves of $Ca_{13.9}Zn_6Ga_{10-y}O_{35}$:0.1$Dy^{3+}$, y$Mn^{4+}$ phosphors doped with various Mn^{4+} concentrations (excited at 266 nm and monitored at 486 nm). (b) The dependence of lifetime and energy transfer efficiency (corresponding to the Dy^{3+} $^4F_{9/2} \rightarrow {}^6H_{15/2}$ transition) in $Ca_{13.9}Zn_6Ga_{10-y}O_{35}$:0.1$Dy^{3+}$, y$Mn^{4+}$ ($y = 0.05, 0.09, 0.12, 0.15, 0.20, 0.25$) on Mn^{4+} concentration.

According to Dexter's energy-transfer model of multipolar interaction and Reisfeld's approximation, the following relation can be given [49,50]

$$\frac{\tau_{Dy}}{\tau_{Dy-Mn}} \propto C^{S/3} \quad (13)$$

where τ_{Dy} and τ_{Dy-Mn} are the lifetimes of Dy^{3+} in the absence and presence of Mn^{4+}, respectively. C is the sum of the concentrations of Dy^{3+} and Mn^{4+}, and $S = 6$, 8 and 10 corresponding to d–d, d–q, and q–q interactions, respectively. Fig. 15 shows the linear fitting of the relationship between $\tau_{Dy}/\tau_{Dy\text{-}Mn}$ and $C^{S/3}$, and the largest values of R^2 with $S = 6$, indicating that the energy transfer from Dy^{3+} to Mn^{4+} occurs *via* d–d interaction.

Fig. 16 shows the CIE chromaticity diagram of (a) CZGO, (b) $Ca_{13.9}Zn_6Ga_{10}O_{35}$:0.1$Dy^{3+}$, (c) $Ca_{13.9}Zn_6Ga_{9.85}O_{35}$:0.1$Dy^{3+}$, 0.15$Mn^{4+}$ excited at 266 nm and (d) $Ca_{14}Zn_6Ga_{9.85}O_{35}$:0.15$Mn^{4+}$ excited at 310 nm. The phosphor CZGO emits deep blue light, of which the chromaticity coordinate is (0.158, 0.062). The chromaticity coordinates of $Ca_{13.9}Zn_6Ga_{10}O_{35}$:0.1$Dy^{3+}$ and $Ca_{13.9}Zn_6Ga_{9.85}O_{35}$:0.1$Dy^{3+}$, 0.15$Mn^{4+}$ with CCTs of 5252 K and 3522 K, with CRIs of 72 and 87, are (0.254, 0.288) and (0.345, 0.275), respectively. Obviously, higher color rendering index (CRI) and lower color temperature are obtained by adding Mn^{4+} ions. Except for the short exciting wavelength, the high color rendering index ($R_a = 87$) and low color temperature 3522 K can well meet the generally lighting.

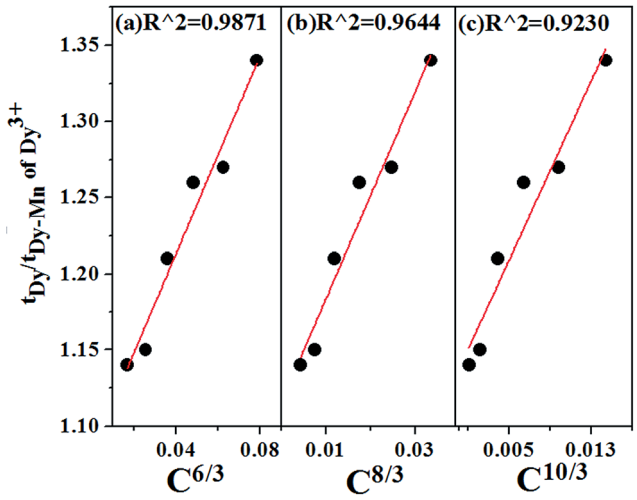

Fig. 15 Dependence of τ_{Dy}/τ_{Dy-Mn} on (a) $C^{6/3}$, (b) $C^{8/3}$ and (c) $C^{10/3}$ in $Ca_{13.9}Zn_6Ga_{10-y}O_{35}$:0.1$Dy^{3+}$, y$Mn^{4+}$ ($y = 0.05, 0.09, 0.12, 0.15, 0.20, 0.25$). The best linear fitting indicates the energy transfer from Dy^{3+} to Mn^{4+} occurs *via* d–d interaction.

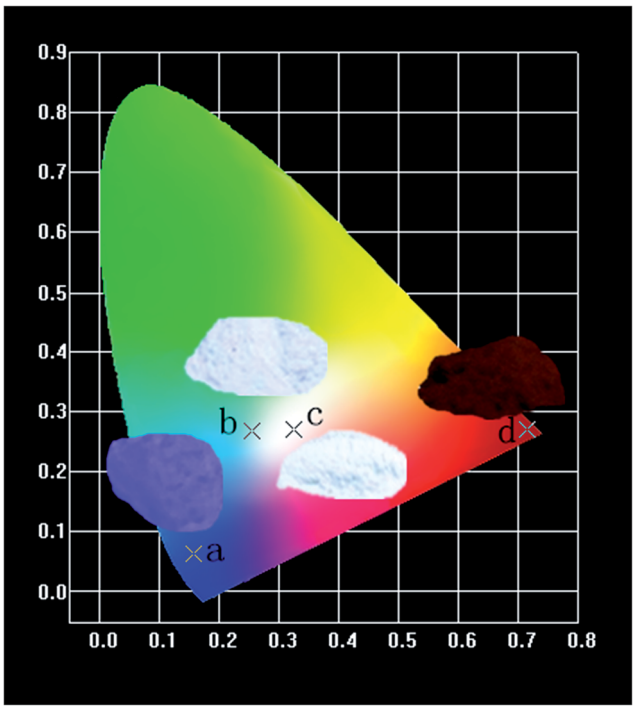

Fig. 16 CIE chromaticity coordinates of (a) CZGO, (b) $Ca_{13.9}Zn_6Ga_{10}O_{35}$:0.1$Dy^{3+}$, (c) $Ca_{13.9}Zn_6Ga_{9.85}O_{35}$:0.1$Dy^{3+}$, 0.15$Mn^{4+}$ excited at 266 nm and (d) $Ca_{14}Zn_6Ga_{9.85}O_{35}$:0.15$Mn^{4+}$ excited at 310 nm in wavelength range 380–800 nm.

4 Conclusion

In summary, strong blue emission band ranging from 370 nm to 500 nm was observed for CZGO host, attributed to the recombination of a donor–acceptor pair (DAP) through a tunneling process. The highest internal and external quantum efficiencies were measured to be 64.4% and 56.2% respectively for CZGO:Mn^{4+}. This external quantum efficiency is the highest one reported for Mn^{4+} doped oxides. The energy transfer processes either from the host to Dy^{3+} or from Dy^{3+} to Mn^{4+} are confirmed and demonstrated arising from dipole–dipole interaction in Dy^{3+}/Mn^{4+} co-doped CZGO, and the emission changes from deep blue to white to deep red according to the different Dy^{3+}/Mn^{4+} concentration ratio, and Furthermore, the warm white emission can be realized with the chromaticity coordinate (0.345, 0.275), CCT 3525 K and CRI 87. The results suggest CZGO:Mn^{4+} phosphors have the potential application as high efficiency red phosphors for solid-state lighting, while Dy^{3+}/Mn^{4+} co-doped CZGO can used as a single-phased white phosphor.

Acknowledgements

Financial supported from the Key Laboratory of Innovation Method and Decision Management System of Guangdong Province, the Research Guangzhou Science (No. 2016201604030035) and Technology Project of Guangdong Province, China (No. 2016201604030027).

References

1 J. H. Chen, W. R. Zhao, N. H. Wang, Y. J. Meng, S. P. Yi, J. He and X. Zhang, *J. Mater. Sci.*, 2016, **51**, 4201–4212.
2 Y. H. Jin, Y. R. Fu, Y. H. Hu, L. Chen, H. Y. Wu, G. F. Ju, M. He and T. Wang, *Powder Technol.*, 2016, **292**, 74–79.
3 T. Murata, T. Tanoue, M. Iwasaki, K. Morinaga and T. Hase, *J. Lumin.*, 2005, **114**, 207–212.
4 M. G. Brik, Y. X. Pan and G. K. Liu, *J. Alloys Compd.*, 2011, **509**, 1452–1456.
5 A. A. Setlur, E. V. Radkov, C. S. Henderson, J.-H. Her, A. M. Srivastava, N. Karkada, M. S. Kishore, N. P. Kumar, D. A. Esram, A. Deshpande, B. Kolodin, L. S. Grigorov and U. Happek, *Chem. Mater.*, 2010, **2**, 4076–4082.
6 G. B. Loutts, M. Warren, L. Taylor, R. R. Rakhimov, H. R. Ries, G. Miller III, M. A. Curley, N. Noginova, N. Kukhtarev, H. J. Caulfeld and P. Venkateswarlu, *Phys. Rev. B: Condens. Matter Mater. Phys.*, 1998, **57**, 3706.
7 Y. Zhydachevskii, D. Galanciak, S. Kobyakov, M. Berkowski, A. Kaminska, A. Suchocki, Y. Zakharko and A. Durygin, *J. Phys.: Condens. Matter*, 2006, **18**, 11385–11396.
8 Y. Zhydachevskii, A. Durygin, A. Suchocki, A. Matkovskii, D. Sugak, P. Bilski and S. Warchol, *Nucl. Instrum. Methods Phys. Res., Sect. B*, 2005, **227**, 545–550.
9 T. Arai and S. Adachi, *Jpn. J. Appl. Phys.*, 2011, **50**, 092401.
10 H. M. Zhu, C. C. Lin, W. Q. Luo, S. T. Shu, Z. G. Liu, Y. S. Liu, J. T. Kong, E. Ma, Y. G. Cao, R. S. Liu and X. Y. Chen, *Nat. Commun.*, 2014, **5**, 4312.
11 T. Takahashi and S. Adachi, *J. Electrochem. Soc.*, 2008, **155**, 183–188.
12 M. H. Du, *J. Mater. Chem. C*, 2014, **2**, 2475.
13 M. G. Brik and A. M. Srivastava, *J. Lumin.*, 2013, **133**, 69–72.
14 M. Y. Peng, X. W. Yin, P. A. Tanner, C. Q. Liang, P. F. Li, Q. Y. Zhang and J. R. Qiu, *J. Am. Ceram. Soc.*, 2013, **96**, 2870–2876.
15 L. Wang, L. Yuan, Y. Xu, R. Zhu, B. Y. Qu, N. Ding, M. Shi, B. Zhang, Y. Chen, Y. Jiang, D. Wang and J. Shi, *Appl. Phys. A*, 2014, **117**, 1777–1783.
16 B. Wang, H. Lin, J. Xu, H. Chen and Y. Wang, *ACS Appl. Mater. Interfaces*, 2014, **6**, 22905–22913.
17 R. Cao, M. Peng, E. Song and J. Qiu, *ECS J. Solid State Sci. Technol.*, 2012, **1**, 123–126.
18 K. Seki, K. Uematsu, K. Toda and M. Sato, *Chem. Lett.*, 2014, **43**, 1213–1215.
19 X. Y. Sun, M. Gu, S. M. Huang, X. L. Liu, B. Liu and C. Ni, *Phys. B*, 2009, **404**, 111–114.
20 S. Y. Istomin, S. V. Chernov, E. V. Antipov and Yu. A. Dobrovolsky, *J. Solid State Chem.*, 2007, **180**, 1882–1888.
21 I. D. Brown, *The Chemical Bond in Inorganic Chemistry. The Bond Valence Model, IUCr Monographs on Crystallography*, Oxford University Press, 2002.
22 R. D. Shannon, *Acta Crystallogr., Sect. A: Cryst. Phys., Diffr., Theor. Gen. Crystallogr.*, 1976, **32**, 751–767.
23 Y. E. Lee, D. P. Norta, C. Park and C. M. Roulean, *J. Appl. Phys.*, 2001, **89**, 1653–1655.
24 K. W. Chang and J. J. Wu, *J. Phys. Chem. B*, 2005, **109**, 13572–13577.
25 L. E. Shea, R. K. Datta and J. J. Brown Jr, *J. Electrochem. Soc.*, 1994, **141**, 1950–1954.
26 I. K. Jeong, H. L. Park and S. I. Mho, *Solid State Commun.*, 1998, **105**, 179–183.
27 J. S. Kim, H. I. Kang, W. Kim, N. J. I. Kim, J. C. Choi, H. L. Park, G. C. Kim, T. W. Kim, Y. H. Hwang, S. I. Mho, M. C. Jung and M. Han, *Appl. Phys. Lett.*, 2003, **82**, 2029–2042.
28 A. M. Srivastava and W. W. Beers, *J. Electrochem. Soc.*, 1996, **143**, L203–L205.
29 Y. Tanabe and S. Sugano, *J. Phys. Soc. Jpn.*, 1954, **9**, 766–779.
30 M. J. Reisfeld, N. A. Matwiyof and L. B. Aspery, *J. Mol. Spectrosc.*, 1971, **39**, 8–20.
31 B. Henderson and G. F. Imbusch, *Optical Spectroscopy of Inorganic Solids*, Clarendon Press, Oxford, UK, 1984.
32 M. G. Brik and A. M. Srivastava, *ECS J. Solid State Sci. Technol.*, 2013, **2**, 148–152.
33 Y. H. Jin, T. H. Hu, H. Y. Wu, H. Duan, L. Chen, Y. R. Fu, D. F. Ju, Z. F. Mu and M. He, *Chem. Eng. J.*, 2016, **288**, 596–607.
34 P. Uylings, A. Raassen and J. Wyart, *J. Phys. B: At. Mol. Phys.*, 1984, **17**, 4103–4126.
35 M. G. Brik and A. M. Srivastava, Ion in Solids, *J. Lumin.*, 2013, **133**, 69–72.
36 V. Bachmann, A. Meijerink and C. Ronda, *J. Lumin.*, 2009, **129**, 1341–1346.
37 Z. G. Xia and R. S. Liu, *J. Phys. Chem. C*, 2012, **116**, 15604–15609.
38 Y. P. Varshni, *Physica*, 1967, **34**, 149–154.

39 J. S. Kim, Y. H. Park, S. M. Kim, J. C. Choi and H. L. Park, *Solid State Commun.*, 2005, **133**, 445–448.
40 Y. L. Huang, J. H. Gana, R. Zhua, X. G. Wang and H. J. Seo, *J. Electrochem. Soc.*, 2011, **158**, 334–J340.
41 W. R. Wang, A. F. Zou, X. Lei, H. P. Gao and Y. L. Mao, *Opt. Mater.*, 2014, **38**, 261–264.
42 Q. Y. Zhang and C. F. Yang, *Appl. Phys. Lett.*, 2007, **91**, 051903.
43 P. I. Paulose, G. Jose, V. Thomas, N. V. Unnikrishnan and M. K. R. Warrier, *J. Phys. Chem. Solids*, 2003, **64**, 841–846.
44 I. R. Martín, V. D. Rodríguez, U. R. Rodríguez-Mendoza, V. Lavín, E. Montoya and D. Jaque, *J. Chem. Phys.*, 1999, **111**, 1191.
45 G. Blasse, *Phys. Lett. A*, 1968, **28**, 444–445.
46 G. Blasse, *Philips Res. Rep.*, 1969, **24**, 131.
47 D. L. Dexter and J. H. Schulman, *J. Chem. Phys.*, 1954, **22**, 1063–1069.
48 Z. Xia, Y. Zhang, M. S. Molokeev and V. V. Atuchin, *J. Phys. Chem. C*, 2013, **117**, 20847–20854.
49 D. L. Dexter and J. H. Schulman, *J. Chem. Phys.*, 1954, **22**, 1063–1070.
50 R. Reisfeld and N. L. Soffer, *J. Solid State Chem.*, 1979, **28**, 391–395.